Progress In Electromagnetics Research B, Vol. 59, 89–102, 2014

Patch and Ground Plane Design of Microstrip Antennas by Material Distribution Topology Optimization

Emadeldeen Hassan*, Eddie Wadbro, and Martin Berggren

Abstract—We use a gradient-based material distribution approach to design conductive parts of microstrip antennas in an efficient way. The approach is based on solutions of the 3D Maxwell's equation computed by the finite-difference time-domain (FDTD) method. Given a set of incoming waves, our objective is to maximize the received energy by determining the conductivity on each Yee-edge in the design domain. The objective function gradient is computed by the adjoint-field method. A microstrip antenna is designed to operate at 1.5 GHz with 0.3 GHz bandwidth. We present two design cases. In the first case, the radiating patch and the finite ground plane are designed in two separate phases, whereas in the second case, the radiating patch and the ground plane are simultaneously designed. We use more than 58,000 design variables and the algorithm converges in less than 150 iterations. The optimized designs have impedance bandwidths of 13% and 36% for the first and second design case, respectively.

1. INTRODUCTION

Microstrip antennas are widely used in various wireless systems because of their many unique and attractive properties [1]. The design of microstrip antennas has benefited from the unrelenting growth in computational power and the increased availability of accurate and efficient methods to numerically solve Maxwell's equations [2]. The traditional design procedure is to define an initial, conceptual layout that is parameterized using a set of design variables, such as the length and width of the patch, the substrate depth, and the position of the feed. If desired, curved boundary shapes can also be designed by parameterizing the positions of control points in a spline, for instance. The performance of the antenna can then be investigated by using either manual parameter variations [3–7] or by employing a numerical optimization approach, where the most common choice is a metaheuristic such as genetic algorithms or particle swarm optimization [8–13].

Such explicit parameterization strategies have been extensively used to design microstrip antennas [3–7, 13–15]. To help the optimization algorithms to find a design in a reasonable time, only a small number of design variables are typically used. Moreover, for antennas mounted over finite ground planes, usually the design of the ground plane is considered in a separate design phase [16–20], which is typically pursued after the design of the antenna patch.

A conceptually different approach to geometry descriptions, which shows promising results [9–11, 21, 22], is to divide the patch surface into small, equally-sized elements. The material property of each element is then directly mapped to the design variables, which will attain binary (0/1) values, typically corresponding to air or conductor. When using a large enough set of such elements, virtually any shape can be obtained through an image representation of the conducting area. However, the use of metaheuristics such as genetic algorithms is computationally intractable for very large dimensions of the design space [23]. To find a suitable design, metaheuristic-based algorithms typically require a number of iterations that is two to three orders of magnitude larger than the number of design variables. For

Received 6 March 2014, Accepted 27 March 2014, Scheduled 1 April 2014
* Corresponding author: Emadeldeen Hassan (emad@cs.umu.se).
The authors are with the Department of Computing Science, Umeå University, Umeå SE-901 87, Sweden.

example, Su et al. [24] used 200 design variables, and their genetic algorithm required 10,000 calls to the Maxwell solver to provide the solution. In another design optimization example, the algorithm developed by Bayraktar et al. [11] called the Maxwell solver 12,500 times to design an artificial magnetic conductor parametrized with 64 design variables. Therefore, only quite crudely shaped geometries can be designed when metaheuristics is used, and design symmetries are often imposed to reduce the dimensions of the design problems.

The *material distribution approach to topology optimization* was originally proposed for structural optimization [25], and it has been successfully extended to many areas in engineering, such as acoustics, optics, and electromagnetics [26–32]. In this approach, a material indicator function p is used to indicate presence, $p = 1$, or absence, $p = 0$, of a material in each of a large number of small elements inside a design domain. But unlike the binary design approach mentioned above, in the material distribution approach, the material indicator function p is allowed to attain intermediate values during the design process (that is, values between 0 and 1, known also as gray values). By the end of the design process, these intermediate values typically vanish, and the final designs have only binary values (0/1). The reason to allow intermediate values is to enable the use of computationally efficient gradient-based optimization algorithms [33]. Such algorithms require derivatives with respect to the design variables of the objective function and the constraints. These derivatives may in many cases be efficiently computed using the adjoint-field method [34–38].

The material distribution approach to topology optimization has been used to design the dielectric parts of patch antennas and dielectric resonator antennas (DRAs) [29, 39]. Further, this technique was recently used to design the metallic radiating elements of different antenna types [30, 31]. In this work, we use the material distribution approach to design the metallic parts of microstrip antennas. We formulate the antenna design problem as an optimization problem, where the objective is to maximize the energy received by the antenna from a given set of far-field sources. The FDTD method is used for the numerical computations [40]. The design variables are directly mapped to the physical conductivities of the Yee-edges inside a specific domain. We use the adjoint-field method [34–38] in order to efficiently calculate the gradient of the objective function. The gradient expression has been derived in the fully discrete case based on the FDTD discretization of Maxwell's equations. Due to the use of the adjoint-field method, the objective function gradient is computed for an arbitrary number of design variables using only two FDTD simulations. The efficiency of the design algorithm makes it possible to simultaneously design both the radiating patch and the ground plane of the antenna.

2. PROBLEM SETUP AND GOVERNING EQUATIONS

The problem setup is schematically shown in Figure 1. A design domain $\Omega \subset \Omega_\infty$ holds a conductivity distribution $\sigma(\mathbf{x})$ that defines the conductive parts of the antenna, with $\mathbf{x}$ representing a point in the design domain. A coaxial transmission line couples signals, through an aperture in the xy plane, to and from the analysis domain Ω_∞. The boundary Γ_{coax} is used to introduce wave energy $W_{\text{in,coax}}$ into the coaxial cable and to measure the wave energy $W_{\text{out,coax}}$ received from the antenna. The coaxial cable has an inner core with diameter d, a metallic shield with diameter D, and is filled with a material with dielectric constant ϵ_c and permeability μ_c. The boundary Γ_{out} represents an outer boundary to the analysis domain, through which wave energies $W_{\text{in},\infty}$ and $W_{\text{out},\infty}$, as illustrated in Figure 1, might enter or leave the analysis domain, respectively.

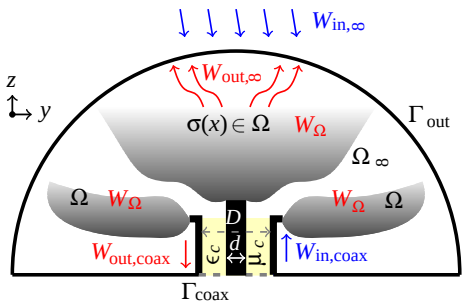

Figure 1. An illustration of the antenna design problem.

The governing equations are the 3D Maxwell's equations in the analysis domain,

$$\frac{\partial}{\partial t}\mu\mathbf{H} + \nabla \times \mathbf{E} = \mathbf{0}, \tag{1a}$$

$$\frac{\partial}{\partial t}\epsilon\mathbf{E} + \sigma\mathbf{E} - \nabla \times \mathbf{H} = \mathbf{0}, \tag{1b}$$

and the 1D transport equation in the coaxial cable,

$$\frac{\partial}{\partial t}\left(V \pm Z_{\mathrm{c}} I\right) \pm c\frac{\partial}{\partial z}\left(V \pm Z_{\mathrm{c}} I\right) = 0, \tag{2}$$

where μ, ϵ, and σ are the permeability, permittivity, and conductivity of the medium; $\mathbf{E}$ and $\mathbf{H}$ are the electric and magnetic fields; V and I are the potential difference and the current inside the coaxial cable; and $c = 1/\sqrt{\mu_c \epsilon_c}$. In expression (2), the term $V \pm Z_{\mathrm{c}} I$ represents two signals that propagate inside the coaxial cable in the negative $(-)$ and in the positive $(+)$ z directions. The signal that propagates in the negative z direction can be used to observe the outgoing energy in the coaxial cable using the integral

$$W_{\mathrm{out,coax}} = \frac{1}{4Z_{\mathrm{c}}}\int_0^T \left(V - Z_{\mathrm{c}} I\right)^2 dt, \tag{3}$$

where $(0, T)$ is the observation time interval. For signals with finite extent in time and for large enough T, the system energy balance illustrated in Figure 1,

$$W_{\mathrm{in,coax}} + W_{\mathrm{in},\infty} = W_{\Omega} + W_{\mathrm{out,coax}} + W_{\mathrm{out},\infty}, \tag{4}$$

where W_{Ω} denotes the ohmic losses in the antenna, can be derived from the system of governing equations and associated boundary and initial conditions.

3. OPTIMIZATION PROBLEM

We design the antenna based on its receiving mode by setting $W_{\mathrm{in,coax}} = 0$ and by imposing a set of incoming waves from the far-field with energy $W_{\mathrm{in},\infty}$. Expression (4) implies that maximizing the energy received by the antenna is equivalent to minimizing the ohmic losses in the antenna W_{Ω} plus the reflected energy $W_{\mathrm{out},\infty}$. We formulate the optimization problem

$$\underset{\sigma(\mathbf{x})\in[\sigma_{\min},\sigma_{\max}]}{\text{maximize}} \quad W_{\mathrm{out,coax}}(\sigma(\mathbf{x})), \tag{5}$$

where $\sigma_{\min}$ and $\sigma_{\max}$ represent physical conductivities of a low-loss dielectric and a good conductor, respectively. Note that unlike the binary (0/1) design problems [9–11, 21, 22], here the design conductivities are allowed to attain any value between $\sigma_{\min}$ and $\sigma_{\max}$ during the design process. In previous work [31], we observed that optimization problem (5) has very low sensitivity for changes in physical conductivities lower than 10^{-4} S/m or greater than 10^{5} S/m. We therefore use the following mapping between the material indicator function $0 \leq p(\mathbf{x}) \leq 1$ and the physical conductivity

$$\sigma(\mathbf{x}) = 10^{(9p(\mathbf{x})-4)}. \tag{6}$$

The use of intermediate conductivity values introduces energy losses in the design domain. Therefore, the solution of problem (5) will be sensitive to the energy loss W_{Ω}. When starting with intermediate conductivities, gradient-based optimization algorithms will quickly drive the solution towards the lossless cases (that is, towards $\sigma_{\min}$ or $\sigma_{\max}$), and generally the obtained designs will have unacceptable performance. We refer to the Appendix for examples. To handle this problem, we use a continuation approach [31], in which we replace $p(\mathbf{x})$ in expression (6) with $\tilde{p}(\mathbf{x}) = K_R * p(\mathbf{x})$, where K_R is an integral operator with support on a disk with radius R. In the topology optimization community, the integral operator K_R is called a filter and is typically used to obtain mesh-independent designs [25]. However, here the main reason to filter the design variables is to control the energy losses inside the design domain. The use of a large filter radius imposes large regions of intermediate conductivities and associated energy losses in the design domain. We start with a radius R_0 and solve problem (5) for a sequence of subproblems, where after partial convergence of a subproblem, we decrease the filter radius by setting $R_n = \gamma R_{n-1}$, where $\gamma < 1$ is a constant filter decrease coefficient. The convergence of a

subproblem is evaluated by measuring the change of the norm of the first order optimality conditions. We record the norm of the first order optimality conditions after 6 iterations of starting a subproblem solution, and the iterations continue until the this norm has decreased by 50% of the recorded value. The algorithm terminates when the radius R_n decreases beyond a small value that we typically choose to be half the smallest numerical grid size. In general, the final design will essentially contain two conductivity values that correspond to $\sigma_{\min}$ and $\sigma_{\max}$, respectively.

4. DISCRETIZATION

We numerically solve the system of governing Equations (1) and (2) by the FDTD method [40] on a uniform grid. The electric field in Maxwell's equations and the potential difference inside the cable are discretized at full time indices, while the magnetic field and the current in the cable are discretized at half time indices. A uniaxial perfectly matched layer (UPML) is used to simulate the open space radiation condition [41].

In the design domain, we define vectors $\mathbf{p}$, $\tilde{\mathbf{p}}$, and $\boldsymbol{\sigma}$ to hold values of p, $\tilde{p}$, and σ, respectively, at each Yee-edge. We formulate the following discrete version of optimization problem (5):

$$\underset{\mathbf{p}\in\mathcal{A}}{\text{maximize}} \quad W^{\Delta}_{\text{out,coax}}(\mathbf{p}). \tag{7}$$

Here $\mathcal{A} = \{\boldsymbol{p} \in [0,1]^M\}$, in which M is the number of Yee-edges in the design domain, and we use the discrete objective function,

$$W^{\Delta}_{\text{out,coax}}(\sigma) = \frac{1}{Z_m}\sum_{n=0}^{N}\left(V^{n+1} - \hat{Z}_{\text{c}} I_z^{n+\frac{1}{2}}\right)^2 \Delta t, \tag{8}$$

where V^{n+1}, $I_z^{n+\frac{1}{2}}$, and $\hat{Z}_{\text{c}}$ are the potential difference, the current, and the characteristic impedance of the discrete coaxial cable model; $Z_{\text{m}} = \sqrt{\mu_c/\epsilon_c}$; N is the total number of time steps required for the simulation to reach steady state; and Δt is the time step used in the FDTD method.

We use the globally convergent method of moving asymptotes (GCMMA) [42] to solve optimization problem (7). The GCMMA is a gradient-based optimization method that is well suited for the mathematical structure of material distribution problems [25, §1.2]. By using the adjoint-field method [34–38] and the FDTD discretization of the governing Equations (1) and (2), we derive (in the fully discrete case) the following expression for the gradient of the objective function (8):

$$\frac{\partial W^{\Delta}_{\text{out,coax}}}{\partial \sigma_i} = -\Delta^3 \sum_{n=1}^{N} E_i^{N-n}\,\frac{E_i^{*\,n-\frac{1}{2}} + E_i^{*\,n+\frac{1}{2}}}{2}\Delta t, \tag{9}$$

where i is the index for an arbitrary Yee-edge inside the design domain; Δ is the spatial discretization step; E_i is the discrete electric field obtained from the FDTD solution to Equations (1) and (2); and E_i^* is a discrete adjoint electric field obtained by solving an adjoint system. The adjoint system is equivalent to an FDTD discretization of Equations (1) and (2). However, in the adjoint system the electric field and the potential difference are discretized at half time indices, while the magnetic field and the current are discretized at full time indices. Moreover, the adjoint system is excited only through the boundary Γ_{coax}, at the bottom of the coaxial cable, using the expression

$$V^{*n-\frac{1}{2}} + \hat{Z}_{\text{c}} I_z^{*\,n-1} = V^{N-n+1} - \hat{Z}_{\text{c}} I_z^{N-n+\frac{1}{2}} \quad \text{for } n = 1,\ldots,N, \tag{10}$$

where $V^{*n-\frac{1}{2}}$ and $I_z^{*\,n-1}$ are the discrete potential difference and the current in the coaxial cable for the adjoint system, respectively. We note that expression (10) imposes the signal that propagates in the cable's positive z direction for the adjoint system to be equal to the time-reversed signal that was propagated in the cable's negative z direction for Equation (2).

5. NUMERICAL RESULTS AND DISCUSSION

We consider the design of a microstrip antenna with the configuration shown in Figure 2. The antenna has a finite ground plane with dimensions $L_g = W_g = 105\,\text{mm}$; a radiating patch with dimensions $L_p = W_p = 75\,\text{mm}$, symmetrically located above the ground plane; and a 6 mm-thick substrate with a dielectric constant 2.62 and loss tangent 0.001 at 2 GHz. A 50 Ohm coaxial cable is connected to the patch area at a point shifted a distance $(-W_p/4,\, 0.0)$ from the patch center. The objective is to design the conductive parts of the microstrip antenna to maximize the energy received in the frequency band 1.35–1.65 GHz.

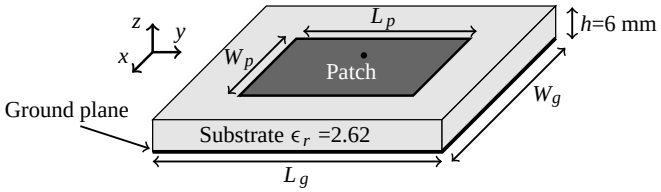

Figure 2. The geometry of the microstrip antenna design problem. A patch area with $L_p = W_p = 75\,\text{mm}$ resides on a 6 mm thick substrate with $\epsilon_r = 2.62$. The inner probe of a 50 Ohm coaxial cable is connected, through a ground plane with $L_g = W_g = 105\,\text{mm}$, to the patch area at a point shifted $(-W_p/4,\, 0.0)$ from the center. The cable's shield is connected to the ground plane.

Since the antenna is designed in its receiving mode, we expect the optimization results to be sensitive to the number of wave sources and their polarizations. In preliminary numerical experiments, we observed that an increase of the number of sources and the use of sources that radiate several field polarizations allowed the algorithm to converge to designs with smaller sizes and better impedance bandwidth (that is, $|S_{11}| < -10\,\text{dB}$ over a wider bandwidth). Therefore, we choose wave sources that generate circularly-polarized plane waves propagating towards the antenna from the sides that correspond to the Cartesian coordinate axes, excluding the negative z direction (Figure 2).

We use a uniform FDTD grid with $\Delta = 0.75\,\text{mm}$, Δt equal 0.98 of the Courant limit, a 10Δ thick UPML, and 10Δ free space separation between the UPML and the antenna. A modulated sinc pulse is used to cover the operational frequency band. The total-field scattered-field formulation is used to implement the plane wave excitation in the FDTD method [40], and the plane waves are synchronized to arrive to the feeding point at the same time.

The FDTD code is implemented to run on Graphics Processing Units (GPUs), using the parallel computing platform CUDA (https://developer.nvidia.com/what-cuda), and double-precision arithmetic is used in all computations. The average simulation time for one FDTD simulation is 220 seconds, and the memory required for gradient computations varies between 3–8.5 GB depending on the design domain size. The conductive sheets are modelled in the FDTD grid using single layers of Yee-faces and are expected to have a mesh-dependent effective thickness of about 0.2Δ [43], which is approximately 0.15 mm.

5.1. Optimization Results

As a first test case, we consider the design of the radiating patch over a fixed square ground plane. The patch area is discretized using 100×100 Yee-faces, which gives a design problem with 20,200 design variables (one conductivity component per Yee-edge). We choose $\mathbf{p}_i = 0.4$ for each i, as an initial design. We use a filter with initial radius $R_0 = 15\,\text{mm}$ and filter decrease coefficient $\gamma = 0.75$. Figure 3 shows the iteration history of the objective function, and also some snapshots of the filtered design variables $\tilde{\mathbf{p}}$ over the patch area, where the black color corresponds to $\sigma_{\max}$ and the white color to $\sigma_{\min}$. In the early stage of the design process, the large filter radius imposes thick gray regions corresponding to intermediate conductivities inside the design domain. As the algorithm proceeds from one subproblem to the next, the thickness of the gray regions decreases, and more details appear inside the design domain. We note the sudden raises in the objective function values between consecutive subproblems (Figure 3). A decrease of the filter radius reduces the amount of imposed losses and allows

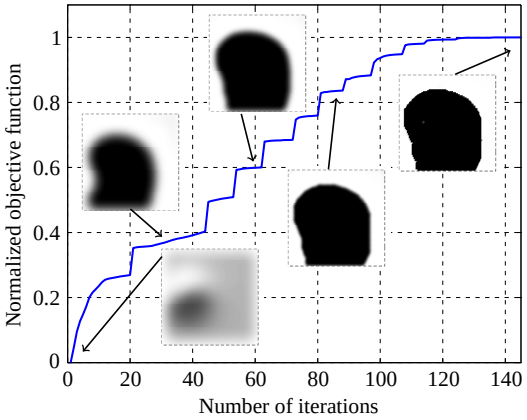

Figure 3. The progress in the normalized objective function and samples of the filtered design variables, $\tilde{\mathbf{p}}$, for the design of the radiating patch over a finite square ground plane.

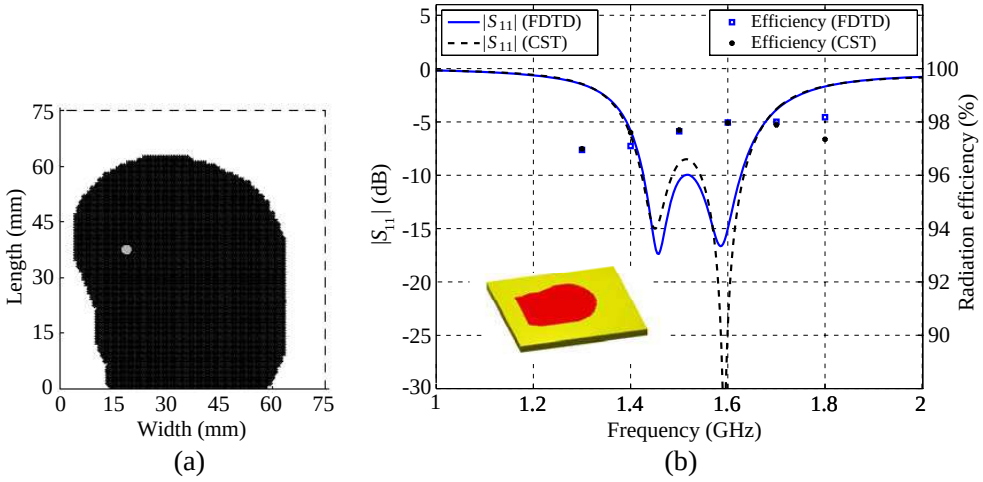

Figure 4. (a) The optimized conductivity distribution over the design domain (patch area) for a finite square ground plane of area $105 \times 105\,\mathrm{mm}^2$. The design domain is $75 \times 75\,\mathrm{mm}^2$ (100×100 Yee-faces). The coaxial cable, marked as a gray circle, is connected at (18.75 mm, 37.5 mm). (b) The reflection coefficient and the radiation efficiency of the antenna.

the optimization algorithm to alter the design variables to maximize the received energy. Without the filter and the systematic continuation approach, the optimization algorithm will generally converge to a design consisting of scattered conducting material that has inferior performance, as demonstrated in the appendix.

The optimization algorithm converged in 145 iterations to the final design shown to the left in Figure 4. Typically, in each iteration the FDTD code is called 3–5 times, where 2 calls are used for computing the objective function gradient and 1–3 calls are used in inner iterations of the GCMMA algorithm to find suitable updates of the design variables. To evaluate the performance of the final design, we use a threshold value $\sigma_{\mathrm{th}} = 10^{-3}\,\mathrm{S/m}$, where conductivities below σ_{th} are mapped to $0\,\mathrm{S/m}$ and values greater than σ_{th} are mapped to $5.8 \times 10^7\,\mathrm{S/m}$. To the right in Figure 4, the reflection coefficient and the radiation efficiency of the final design are computed with our FDTD code and cross-verified using the CST Microwave Studio software, employing adaptive mesh refinement and modelling the patch and the ground plane as 0.15 mm thick sheets with conductivity $5.8 \times 10^7\,\mathrm{S/m}$. A reason for the slight difference in the computed results could be the difference in geometry description between the two methods. The final design has a reflection coefficient below $-10\,\mathrm{dB}$ over the frequency band 1.42–1.62 GHz, with a small exception around the frequency 1.52 GHz, where the reflection coefficient

hits the −10 dB line. The antenna has on average a radiation efficiency of 97.5% over the frequency band 1.42–1.62 GHz.

Figure 5 shows the surface current amplitudes, computed with our FDTD code, over the antenna at frequencies 1.4, 1.5, and 1.6 GHz. These results have been cross-verified with the CST package, but for brevity we include only our FDTD code's results. At 1.4 and 1.5 GHz, most of the surface current on the patch area is concentrated along its four boundary edges (the first row in the figure), whereas at 1.6 GHz the surface current is essentially concentrated along the edges parallel to the x axis. Further,

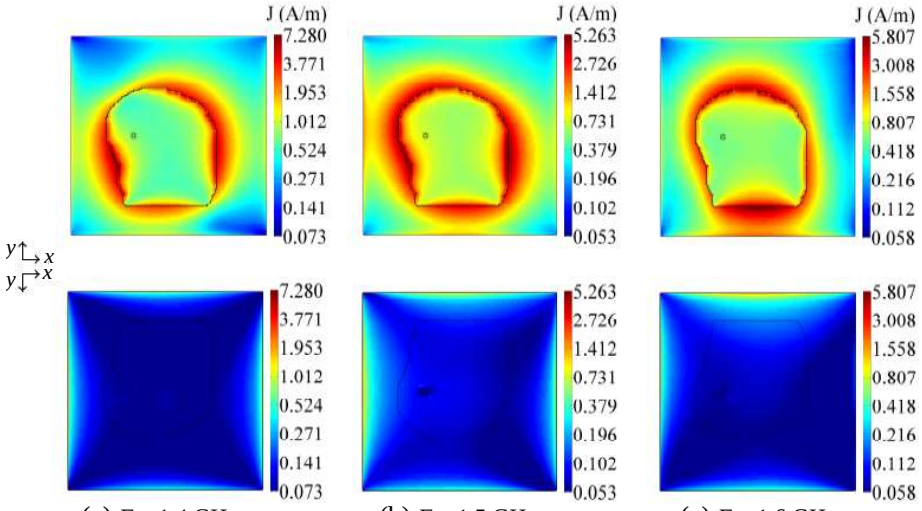

(a) F = 1.4 GHz (b) F = 1.5 GHz (c) F = 1.6 GHz

Figure 5. Surface currents over the radiating patch given in Figure 4 and a 105 × 105 mm^2 ground plane at 1.4, 1.5, and 1.6 GHz. The first row is the surface current seen from the positive z axis, and the second row is the surface current seen from the negative z axis.

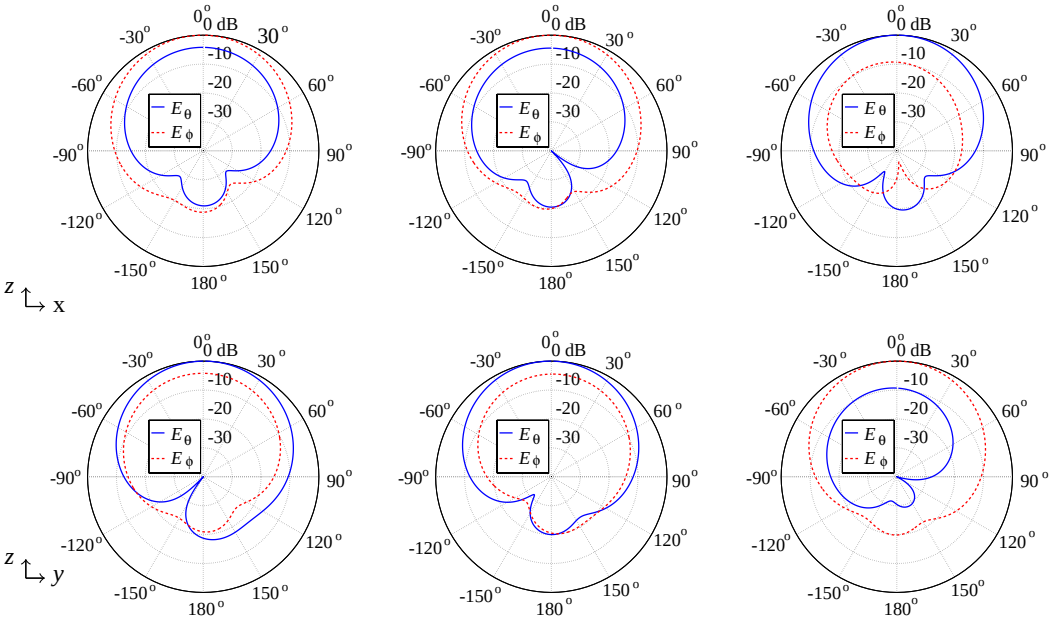

(a) F = 1.4 GHz (b) F = 1.5 GHz (c) F = 1.6 GHz

Figure 6. Simulated radiation patterns at (a) 1.4, (b) 1.5, and (c) 1.6 GHz for the microstrip antenna with the radiating patch given in Figure 4 and a 105 × 105 mm^2 ground plane.

the surface current below the ground plane (the second row) has relatively small values compared to the current above the ground, and the maximum values occur at the ground plane edges. Figure 6 shows the simulated radiation patterns at 1.4, 1.5, and 1.6 GHz. The current distribution on the patch at 1.4 and 1.5 GHz results in two orthogonal far-field components that have on average a difference of 5 dB at the positive z axis, however, at 1.6 GHz the difference is approximately 10 dB. Further, the finite ground plane results in almost a 20 dB front-to-back ratio at the three frequencies. We emphasize that the goal of the current work is to design the antenna to maximize any available received energy in the frequency band 1.35–1.65 GHz, and we do not impose requirements on the far-field polarization nor the radiation pattern.

As a second test case, we fix the patch to be the design given in Figure 4, and we use the optimization algorithm to redesign the $105 \times 105\,\text{mm}^2$ ground plane, which is discretized in the FDTD grid using

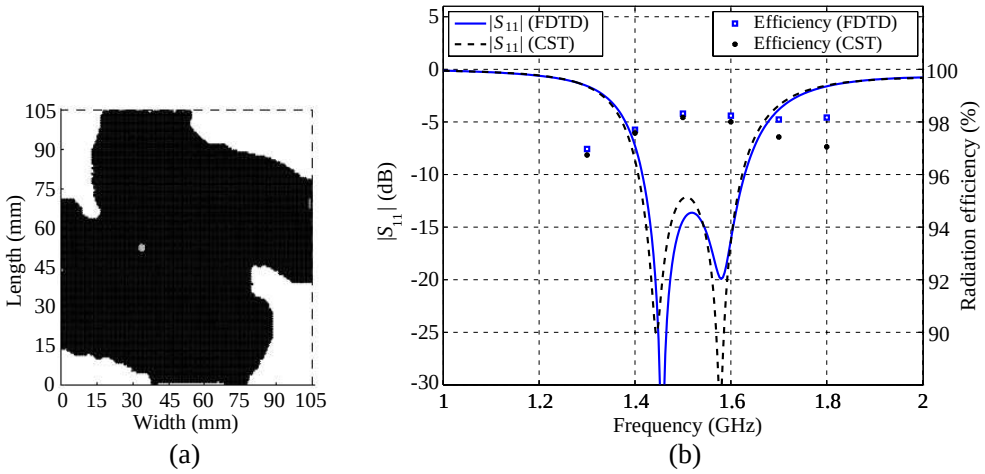

Figure 7. (a) The optimized conductivity distribution over the ground plane when the design given in Figure 4 is used as the radiating patch. The design domain has 38,076 design variables. The coaxial probe, marked as a gray circle, is connected at (33.75 mm, 52.5 mm). (b) The reflection coefficient and the radiation efficiency of the antenna.

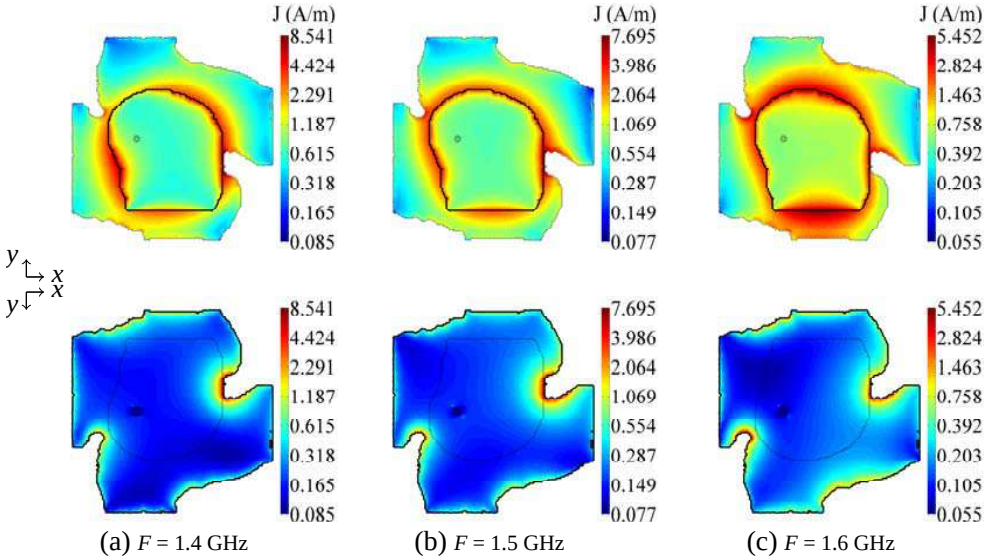

Figure 8. Surface currents over the radiating patch given in Figure 4 and the ground plane given in Figure 7 at 1.4, 1.5, and 1.6 GHz. The first row is the surface current seen from the positive z axis, and the second row is the surface current seen from the negative z axis.

140 × 140 Yee-faces (39,480 Yee-edges). To guarantee a well-defined support for the coaxial cable connection, an area of 19.5 × 19.5 mm^2 around the coaxial feed is excluded from the design and fixed to be a conductor. The design problem has in total 38,076 design variables; that is, 39,480 on the ground plane minus 1,404 of the fixed area around the coaxial cable. We use the same settings as for the first design case, except that the initial value of the design variables is $\mathbf{p}_i = 0.8$ (to make the initial conductivity over the ground plane closer to a conductor than to free space). The algorithm converged in 133 iterations to the final design shown to the left in Figure 7. The reflection coefficient and the radiation efficiency of the antenna are shown in the same figure to the right. The antenna has a reflection coefficient below −10 dB over the frequency band 1.42–1.62 GHz, and the value at 1.52 GHz decreased, compared to the previous case, to −13.8 dB. The surface currents over the antenna at 1.4, 1.5, and 1.6 GHz are shown in Figure 8. The surface current distribution over the patch is similar to the one in Figure 5. However, below the ground plane, the surface current amplitudes are higher along the ground plane edges compared to the case of the square ground plane. The front-to-back ratio of the new antenna is reduced to about 15 dB at the three frequencies 1.4, 1.5 and 1.6 GHz, as shown in

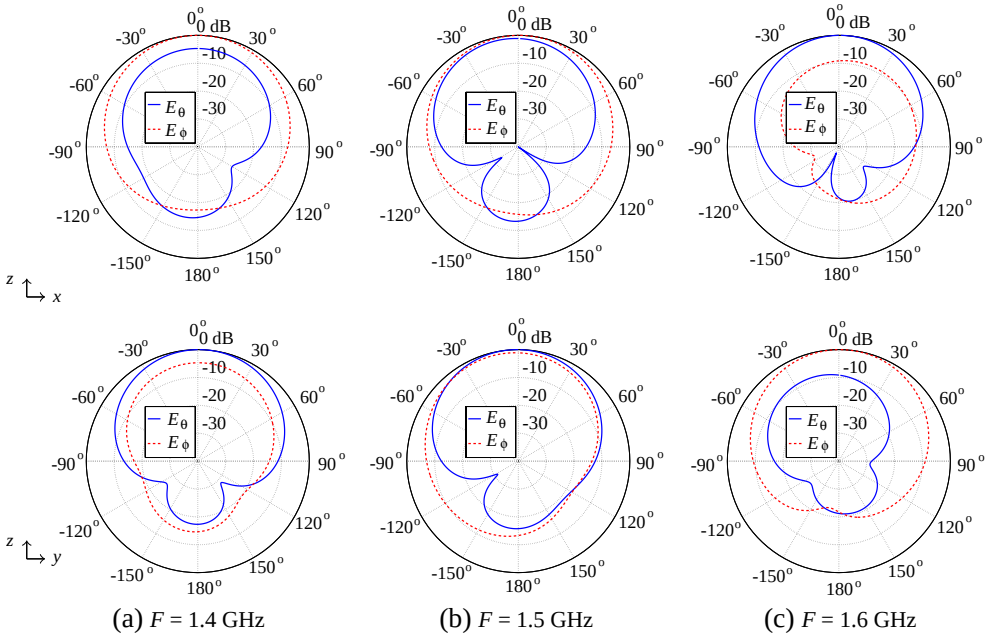

Figure 9. Simulated radiation patterns at (a) 1.4, (b) 1.5, and (c) 1.6 GHz for the microstrip antenna with the radiating patch given in Figure 4 and the ground plane given in Figure 7.

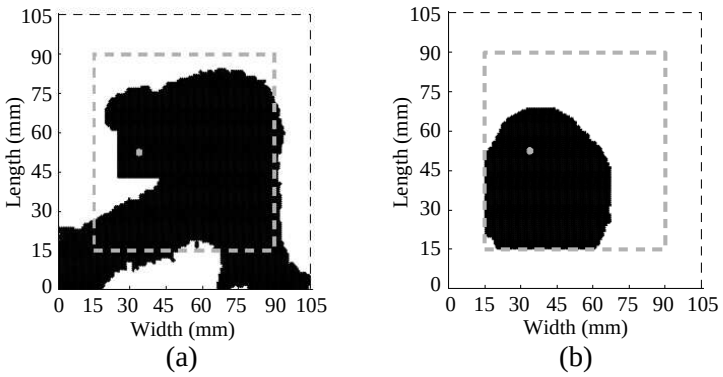

Figure 10. The optimized conductivity distribution over (a) the ground plane and (b) the patch area when the radiating patch and the ground plane are simultaneously designed. The design problem has in total 58,276 design variables. The location of the coaxial probe is marked by a gray circle.

Figure 9, due to the smaller size of the ground plane.

As a final test case, we consider the simultaneous design of the radiating patch and the ground plane. We use the same settings as for the previous two test cases concerning the filter, the initial values of the design variables, and the fixed conductive area $19.5 \times 19.5\,\mathrm{mm}^2$ in the ground plane around the coaxial cable. The design problem has in total 58,276 design variables. The optimization algorithm converged, in 125 iterations, to the final design shown in Figure 10. Figure 11 shows the reflection coefficient and the radiation efficiency of the obtained design computed with our FDTD code and with the CST package. The microstrip antenna has a reflection coefficient below $-10\,\mathrm{dB}$ over the frequency band 1.26–1.83 GHz; that is, the design has an impedance bandwidth of 36.8%. Figure 12 illustrates the surface current distribution at 1.4, 1.5, and 1.6 GHz over the designed conductive parts. We note the higher relative amplitudes of the surface current below the ground plane, especially at the lower frequencies, which indicates the higher influence of the the ground plane in the antenna radiation. Figure 13 shows the simulated radiation patterns at 1.4, 1.5, and 1.6 GHz. The large values of the surface current below the ground plane increase the radiation below the antenna, and the front-to-back ratio is around 5 dB at the three frequencies. Moreover, the antenna has essentially dual-polarized far-field patterns in the boresight direction.

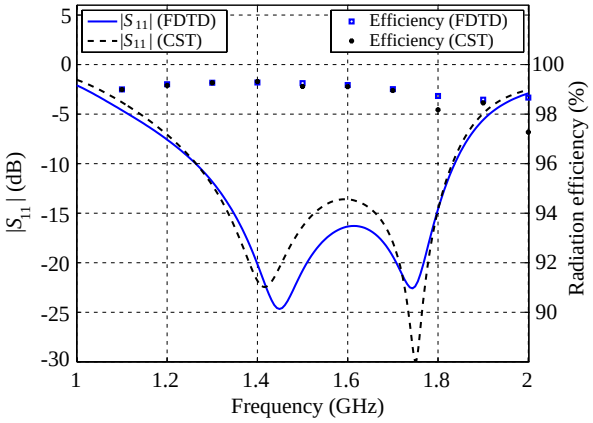

Figure 11. The reflection coefficient and the radiation efficiency of the designs given in Figure 10.

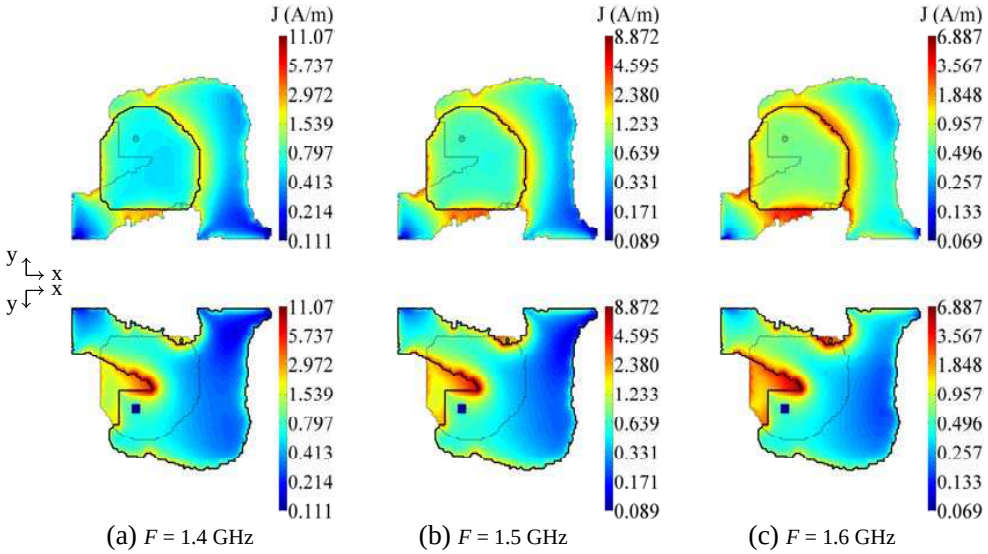

(a) $F = 1.4$ GHz (b) $F = 1.5$ GHz (c) $F = 1.6$ GHz

Figure 12. Surface currents over the radiating patch and the ground plane given in Figure 10 at 1.4, 1.5, and 1.6 GHz. The first row is the surface current seen from the positive z axis, and the second row is the surface current seen from the negative z axis.

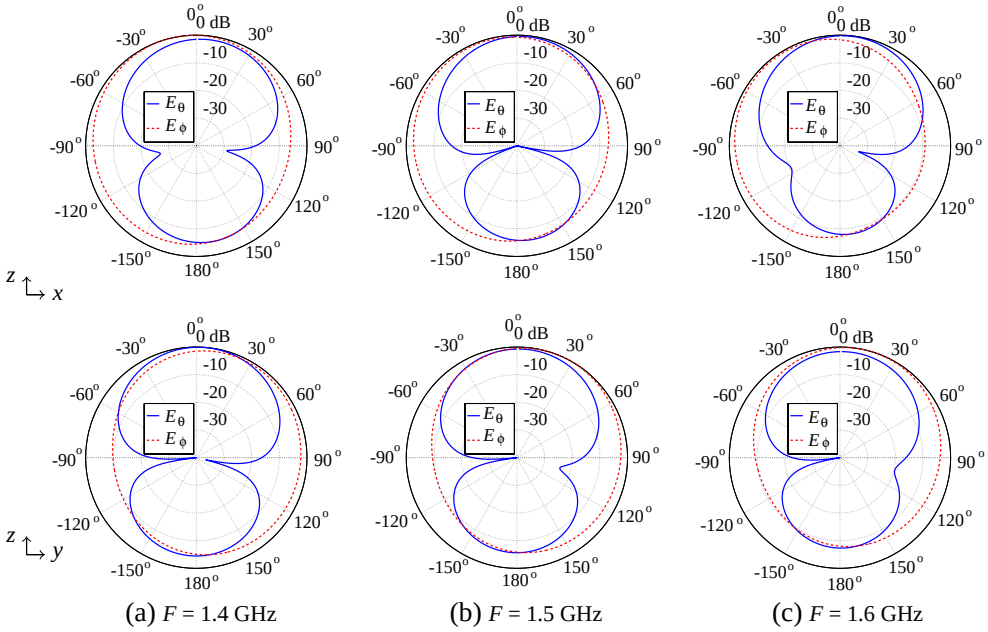

Figure 13. The simulated radiation patterns at (a) 1.4, (b) 1.5, and (c) 1.6 GHz for the microstrip antenna with the radiating patch and the ground plane given in Figure 10.

6. CONCLUSIONS

By relying on a gradient-based material distribution optimization algorithm in combination with derivative calculations based on the adjoint-field method, we are able to optimize the metallic parts of microstrip antennas in a computationally efficient way. The number of iterations in the algorithm does not seem to grow much when the number of design variables are increased, in contrast to standard approaches based on metaheuristics, which typically require a number of iterations that is two to three orders of magnitude greater than the number of design variables. Thus, we are able to work with a dense pixel-based representation of the geometry, which leads to non-intuitive antenna designs, while keeping the number of design iterations well below 200, even when the number of design variables are as high as almost 60,000. The current work focuses on designs that maximize the *received* energy regardless of the wave source's polarizations. Thus, we have no direct control over the *transmitted* far-field pattern. Nevertheless, in the last test case, we achieved a dual-polarized far-field pattern of the antenna in the boresight direction, although we did not explicitly enforce this condition in the optimization. Adding explicit requirements, on the far-field patterns, in the optimization could be a suitable subject for future work.

ACKNOWLEDGMENT

This work is supported financially by the Swedish Research Council. The computations were performed on resources provided by the Swedish National Infrastructure for Computing (SNIC) at the center for scientific and technical computing at Lund University (Lunarc) and at the High Performance Computing Center North (HPC2N) at Umeå University.

APPENDIX A. FILTERING EFFECT

To demonstrate the effectiveness of the filter and the continuation approach in the design process, we show two results obtained by the optimization algorithm without the use of the systematic continuation approach. In the first example, Design I, we use the algorithm to design the radiating patch over the

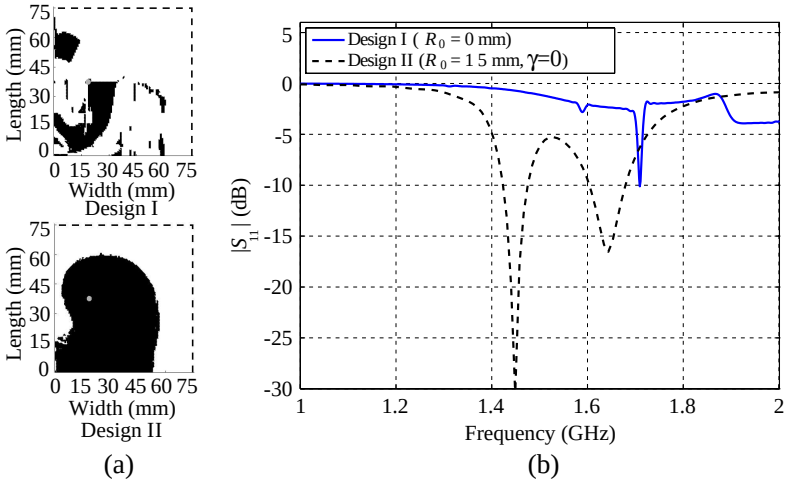

Figure A1. An illustration of the filtering effect on the design. (a) Design I, obtained with no filtering, Design II, obtained by using a filter only for the first subproblem. (b) The reflection coefficient of Design I and Design II.

square ground plane, using the same settings as those for the design in Figure 4, but without the use of a filter (that is, with $R_0 = 0\,\text{mm}$). In the second example, Design II, the filter is removed after the convergence of the first subproblem (that is, using $R_0 = 15\,\text{mm}$ and $\gamma = 0$). Figure A1 shows the resulting designs and their corresponding reflection coefficients computed by our FDTD code. The design algorithm converged in 10 iterations to Design I, which consists of a group of isolated conductive parts that has a reflection coefficient higher than $-3\,\text{dB}$ over the whole frequency band of interest. For Design II, the algorithm converged in 30 iterations, and the reflection coefficient is below $-10\,\text{dB}$ only over the two separated frequency bands 1.42–1.47 GHz and 1.6–1.68 GHz. We conclude that the systematic continuation approach is a crucial component in order for our method to produce antennas with satisfactory performance.

REFERENCES

1. Balanis, C. A., *Antenna Theory: Analysis and Design,* 3rd edition, Wiley-Interscience, 2005.
2. Sadiku, M. N., *Numerical Techniques in Electromagnetics*, 2nd edition, CRC Press, 2001.
3. Chung, K. L. and A. Mohan, "A systematic design method to obtain broadband characteristics for singly-fed electromagnetically coupled patch antennas for circular polarization," *IEEE Trans. Antennas Propag.*, Vol. 51, No. 12, 3239–3248, 2003.
4. Yang, S. S., K.-F. Lee, A. A. Kishk, and K.-M. Luk, "Design and study of wideband single feed circularly polarized microstrip antennas," *Progress In Electromagnetics Research*, Vol. 80, 45–61, 2008.
5. Kaymaram, F. and L. Shafai, "Enhancement of microstrip antenna directivity using double-superstrate configurations," *Can. J. Elect. Comput. E*, Vol. 32, No. 2, 77–82, 2007.
6. Malekpoor, H. and S. Jam, "Miniaturised asymmetric E-shaped microstrip patch antenna with folded-patch feed," *IET Microw. Antennas Propag.*, Vol. 7, No. 2, 85–91, 2013.
7. Kasabegoudar, V. G. and K. J. Vinoy, "Broadband suspended microstrip antenna for circular polarization," *Progress In Electromagnetics Research*, Vol. 90, 353–368, 2009.
8. Johnson, J. and V. Rahmat-Samii, "Genetic algorithms in engineering electromagnetics," *IEEE Antennas Propag. Mag.*, Vol. 39, No. 4, 7–21, 1997.
9. Choo, H., A. Hutani, L. Trintinalia, and H. Ling, "Shape optimisation of broadband microstrip antennas using genetic algorithm," *Electron. Lett.*, Vol. 36, No. 25, 2057–2058, 2000.

10. Villegas, F., T. Cwik, Y. Rahmat-Samii, and M. Manteghi, "A parallel electromagnetic genetic-algorithm optimization (EGO) application for patch antenna design," *IEEE Trans. Antennas Propag.*, Vol. 52, No. 9, 2424–2435, Sep. 2004.
11. Bayraktar, Z., M. Komurcu, J. Bossard, and D. Werner, "The wind driven optimization technique and its application in electromagnetics," *IEEE Trans. Antennas Propag.*, Vol. 61, No. 5, 2745–2757, 2013.
12. Afshinmanesh, F., A. Marandi, and M. Shahabadi, "Design of a single-feed dual-band dual-polarized printed microstrip antenna using a boolean particle swarm optimization," *IEEE Trans. Antennas Propag.*, Vol. 56, No. 7, 1845–1852, Jul. 2008.
13. Griths, L., C. Furse, and Y. C. Chung, "Broadband and multiband antenna design using the genetic algorithm to create amorphous shapes using ellipses," *IEEE Trans. Antennas Propag.*, Vol. 54, No. 10, 2776–2782, Oct. 2006.
14. Uchida, N., S. Nishiwaki, K. Izui, M. Yoshimura, T. Nomura, and K. Sato, "Simultaneous shape and topology optimization for the design of patch antennas," *3rd European Conference on Antennas and Propagation*, 103–107, Mar. 2009.
15. Toivanen, J., R. Mäkinen, J. Rahola, S. Järvenpää, and P. Ylä-Oijala, "Gradient-based shape optimisation of ultra-wideband antennas parameterised using splines," *IET Microw. Antennas Propag.*, Vol. 4, No. 9, 1406–1414, 2010.
16. Noghanian, S. and L. Shafai, "Control of microstrip antenna radiation characteristics by ground plane size and shape," *IEE Proc. on Microw. Antennas Propag.*, Vol. 145, No. 3, 207–212, 1998.
17. Wong, K.-L., C.-L. Tang, and J.-Y. Chiou, "Broadband probe-fed patch antenna with a W-shaped ground plane," *IEEE Trans. Antennas Propag.*, Vol. 50, No. 6, 827–831, 2002.
18. El-Deen, E., S. Zainud-Deen, H. Sharshar, and M. A. Binyamin, "The effect of the ground plane shape on the characteristics of rectangular dielectric resonator antennas," *IEEE AP-S Int. Symp.*, 3013–3016, 2006.
19. Best, S., "The significance of ground-plane size and antenna location in establishing the performance of ground-plane-dependent antennas," *IEEE Antennas Propag. Mag.*, Vol. 51, No. 6, 29–43, 2009.
20. Mandal, K. and P. Sarkar, "High gain wide-band U-shaped patch antennas with modied ground planes," *IEEE Trans. Antennas Propag.*, Vol. 61, No. 4, 2279–2282, 2013.
21. Modiri, A. and K. Kiasaleh, "Efficient design of microstrip antennas for SDR applications using modified PSO algorithm," *IEEE Trans. Magn.*, Vol. 47, 1278–1281, May 2011.
22. Cismasu, M. and M. Gustafsson, "Antenna bandwidth optimization by genetic algorithms with single frequency simulation," *7th European Conference on Antennas and Propagation*, 2781–2782, Gothenburg, Sweden, Apr. 2013.
23. Sigmund, O., "On the usefulness of non-gradient approaches in topology optimization," *Struct. Multidiscip. Optim.*, Vol. 43, 589–596, 2011.
24. Su, D. Y., D.-M. Fu, and D. Yu, "Genetic algorithms and method of moments for the design of PIFAs," *Progress In Electromagnetics Research Letters*, Vol. 1, 9–18, 2008.
25. Bendsøe, M. P. and O. Sigmund, *Topology Optimization — Theory, Methods, and Applications*, Springer, 2003.
26. Wadbro, E., *Topology Optimization for Wave Propagation Problems*, Ph.D. Thesis, Division of Scientic Computing, Uppsala University, Uppsala, Sweden, 2009.
27. Jensen, J. and O. Sigmund, "Topology optimization for nano-photonics," *Laser Photon. Rev.*, Vol. 5, No. 2, 308–321, 2011.
28. Dyck, D. and D. Lowther, "Automated design of magnetic devices by optimizing material distribution," *IEEE Trans. Magn.*, Vol. 32, No. 3, 1188–1193, May 1996.
29. Kiziltas, G., D. Psychoudakis, J. Volakis, and N. Kikuchi, "Topology design optimization of dielectric substrates for bandwidth improvement of a patch antenna," *IEEE Trans. Antennas Propag.*, Vol. 51, No. 10, 2732–2743, Oct. 2003.
30. Erentok, A. and O. Sigmund, "Topology optimization of sub-wavelength antennas," *IEEE Trans. Antennas Propag.*, Vol. 59, No. 1, 58–69, Jan. 2011.

31. Hassan, E., E. Wadbro, and M. Berggren, "Topology optimization of UWB monopole antennas," *7th European Conference on Antennas and Propagation*, 1429–1433, Gothenburg, Sweden, Apr. 2013.
32. Nomura, T., M. Ohkado, P. Schmalenberg, J. Lee, O. Ahmed, and M. Bakr, "Topology optimization method for microstrips using boundary condition representation and adjoint analysis," *2013 European Microwave Conference*, 632–635, Oct. 2013.
33. Nocedal, J. and S. Wright, *Numerical Optimization,* Springer, 1999.
34. Gustafsson, M. and S. He, "An optimization approach to two-dimensional time domain electromagnetic inverse problems," *Radio Science*, Vol. 35, 525–536, Mar. 2000.
35. Chung, Y.-S., C. Cheon, I.-H. Park, and S.-Y.Hahn, "Optimal design method for microwave device using time domain method and design sensitivity analysis. II. FDTD case," *IEEE Trans. Magn.*, Vol. 37, No. 5, 3255–3259, Sep. 2001.
36. Bondeson, A., Y. Yang, and P. Weinerfelt, "Shape optimization for radar cross sections by a gradient method," *Int. J. Num. Meth. Eng.*, Vol. 61, No. 5, 687–715, 2004.
37. Abenius, E. and B. Strand, "Solving inverse electromagnetic problems using FDTD and gradient-based minimization," *Int. J. Num. Meth. Eng.*, Vol. 68, No. 6, 650–673, 2006.
38. Nikolova, N., H. Tam, and M. Bakr, "Sensitivity analysis with the FDTD method on structured grids," *IEEE Trans. Microw. Theory Tech.*, Vol. 52, No. 4, 1207–1216, Apr. 2004.
39. Nomura, T., K. Sato, K. Taguchi, T. Kashiwa, and S. Nishiwaki, "Structural topology optimization for the design of broadband dielectric resonator antennas using the finite difference time domain technique," *Int. J. Num. Meth. Eng.*, Vol. 71, 1261–1296, 2007.
40. Taflove, A. and S. Hagness, *Computational Electrodynamics: The Finite-difference Time-domain Method*, 3rd edition, Artech House, 2005.
41. Gedney, S., "An anisotropic perfectly matched layer-absorbing medium for the truncation of FDTD lattices," *IEEE Trans. Antennas Propag.*, Vol. 44, No. 12, 1630–1639, Dec. 1996.
42. Svanberg, K., "A class of globally convergent optimization methods based on conservative convex separable approximations," *SIAM J. Optim.*, Vol. 12, No. 2, 555–573, 2002.
43. Waldschmidt, G. and A. Taflove, "The determination of the effective radius of a filamentary source in the FDTD mesh," *IEEE Microw. Guided Wave Lett.*, Vol. 10, No. 6, 217–219, 2000.